ACS OMEGA

Open Access

http://pubs.acs.org/journal/acsodf

Article

Design and Synthesis of Quinoxaline Hybrids as Modulators of HIF-1a, VEGF, and p21 for Halting Colorectal Cancer

Mohammed Salah Ayoup,* Ahmed R. Rabee, Hamida Abdel-Hamid, Adel Amer,* Marwa M. Abu-Serie, Samah Ashraf, Doaa A. Ghareeb, Rabab S. Ibrahim, Mohammed B. Hawsawi, Amr Negm, and Magda M. F. Ismail

Cite This: *ACS Omega* 2024, 9, 24643−24653

Read Online

ACCESS | Metrics & More | Article Recommendations | Supporting Information

ABSTRACT: A library of 16 3-benzyl-N^1-substituted quinoxalin-2-ones was synthesized as N^1-substituted quinoxalines and quinoxaline-triazole hybrids via click reaction. These compounds were tested for their anticancer activity via MTT assay on HCT-116 and normal colonocyte cell lines to assess their cytotoxic potentials and safety profiles. Overall, compounds **6**, **9**, **14**, and **20** were found to be promising anticolorectal cancer agents; they exhibited remarkable cytotoxicity (IC_{50} 0.05−0.07 μM) against HCT-116 cells within their safe doses (EC100) on normal colon cells. Their pronounced anticancer activities were observed as severe morphological alterations and shrinkage of the treated cancer cells. Besides, qRT-PCR analysis was conducted showing the potential of the promising hits to downregulate HIF-1a, VEGF, and BCL-2 as well as their ability to enhance the expression of proapoptotic genes p21, p53, and BAX in HCT-116 cells. *In silico* prediction revealed that most of our compounds agree with Lipinski and Veber parameters of rules, in addition to remarkable medicinal chemistry and drug-likeness parameters with no CNS side effects. Interestingly, docking studies of the compounds in the VEGFR-2' active site showed significant affinity toward the essential amino acids, which supported the biological results.

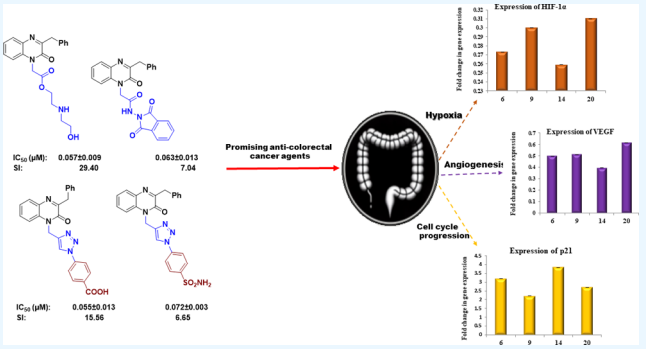

1. INTRODUCTION

Colorectal cancer (CRC) is a malignant tumor that originates in the colon or rectum. It is one of the most common types of cancer worldwide and a significant cause of cancer-related mortality. It is acknowledged as one of the metabolic cancers and is rated as the second most common cancer in women and the third most prevalent cancer in men.[1] Vascular endothelial growth factor (VEGF) is eminently expressed in cancer cells under diverse circumstances, e.g., acidosis, hypoxia, mechanical stress, and unbalanced tumor suppressor genes.[2,3] As a vascular endothelial cell-specific mitogen, VEGF produced by malignant cells persuades angiogenesis[4] by promoting the proliferation and division of matrix endothelial cells, augments vascular permeability, boosts tumor metastasis, and acts precisely on tumor cells to encourage tumor cell growth.[5] The synthesis of VEGF and its receptors is regulated by hypoxia-inducible factor 1-α (HIF-1α). HIF-1 is a heterodimer involved in embryonic development, tumor growth, metastasis, and apoptosis; it is sensitive to the fluctuations in oxygen levels.[6] Under hypoxia, HIF-1α is stabilized and enters the nucleus, where it binds to the hypoxia-responsive elements (HREs) to activate the transcription of many genes related to tumor aggressiveness and chemoresistance.[7,8]

Quinoxaline is a crucial component (**I**−**IV**) in drugs used to destroy cancerous cells, which support a great future in medicinal chemistry.[9−11] **I** and **II** recently were reported as VEGFR-2 inhibitors.[12] *N*-benzyl-4-(2-(3-methyl-2-oxoquinoxalin-1(2*H*)-yl)acetamido) (**III**) was reported as more potent cytotoxic (IC_{50} 2.20 μM) compared to doxorubicin (IC_{50} 9.63 μM) and sorafenib (IC_{50} 9.40 μM) against the HCT-116 cell line. It potently inhibited VEGFR-2 at a lower IC_{50} value of 1.09 μM compared to sorafenib (IC_{50} 1.27 μM).[13] Hybridization of quinoxaline with other anticancer pharmacophores like triazole[14,15] has a significant importance and application in cancer control; the N^1-1,3,4-triazolo-quinoxaline derivative (**IV**, IC_{50} 0.037 μM) showed more potent VEGFR-2 inhibitory activity than sorafenib (IC_{50} 0.045 μM).[8]

Drawing from the previously described findings and in keeping with our studies on anticancer drugs,[12,16] we concentrated on the synthesis of novel quinoxalines and assessed

Received: February 2, 2024
Revised: April 30, 2024
Accepted: May 14, 2024
Published: May 29, 2024

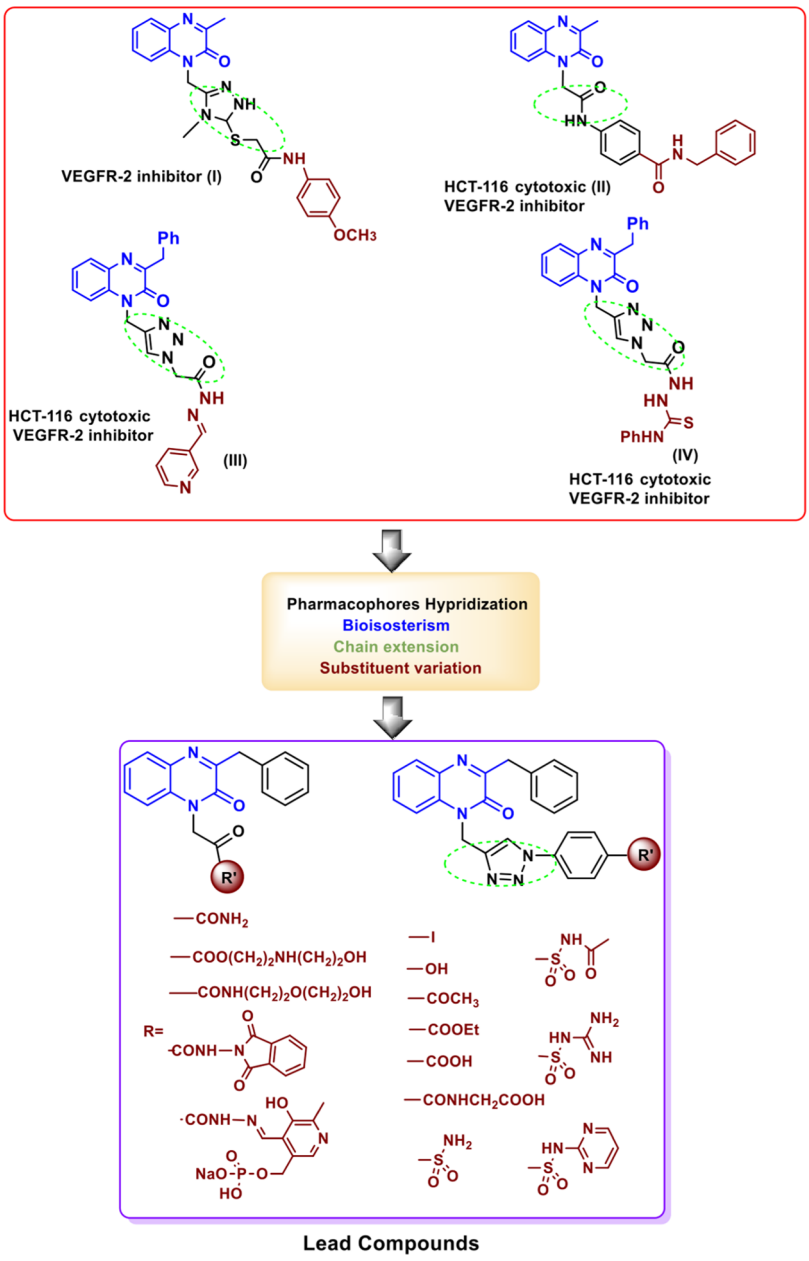

Figure 1. Rational of the target-based 3-benzylquinoxaline derivatives.

their ability to halt colorectal cancer as one of the resistant types of cancer. Our rationale is based on employing quinoxaline to discover a new class of quinoxaline-2(1H)-one-based anticancer agents targeting VEGFR-2 as inhibitors like the reported ones, **III** and **IV** (Figure 1). Moreover, another strategy such as chain extension was followed, searching for the critical distance linking N^1 of quinoxaline to various bioactive moieties. Pharmacophore hybridization (quinoxaline, triazole, and carboxamide) and substituent variation were applied too. Thus, a novel series of N^1-substituted quinoxaline and quinoxaline-triazole hybrids were designed and synthesized. Their cytotoxicity against HCT-116 and normal colonocyte cell lines was evaluated. Afterward, mechanistic study of the promising hits was performed by targeting several signaling machinery such as the expression of HIF, VEGF, and p21 proteins. *In silico* molecular docking and *ADME* prediction were determined as well.

2. RESULTS AND DISCUSSION

2.1. Chemistry. Herein, our work targeted on the preparation of novel 3-benzylquinoxalin-2-one derivatives via alkylation reaction utilizing different alkylating reagents, namely, Sanger's reagent, propargyl bromide, and ethyl bromoacetate to afford the *N*-dinitrophenylquinoxaline derivative **2**, the *N*-alkynylquinoxaline derivative **3**, and the quinoxalinyl ethyl acetate derivative **4**, respectively (Scheme 1). The structure of the synthesized compounds **2**, **3**, and **4** was confirmed using spectroscopic data; compounds **2** and **4** were prepared as described in the previous work.[17−19] The structure of compound **3** was confirmed by its IR spectrum, which showed a strong band at ν (cm^{-1}): 3260 corresponds to the Csp-H stretch, and the 2121 band corresponds to the acetylinic bond C≡C, and its ^{13}C NMR spectrum showed peaks at δ_C: 77.9, 75.3 (C≡C).

The functionalization of compound **4** was accomplished by different protocols where treatment of **4** with aqueous ammonia

https://doi.org/10.1021/acsomega.4c01075
ACS Omega 2024, 9, 24643−24653

Scheme 1. Synthesis of *N*-Substituted 3-Benzylquinoxaline Derivatives 2−4

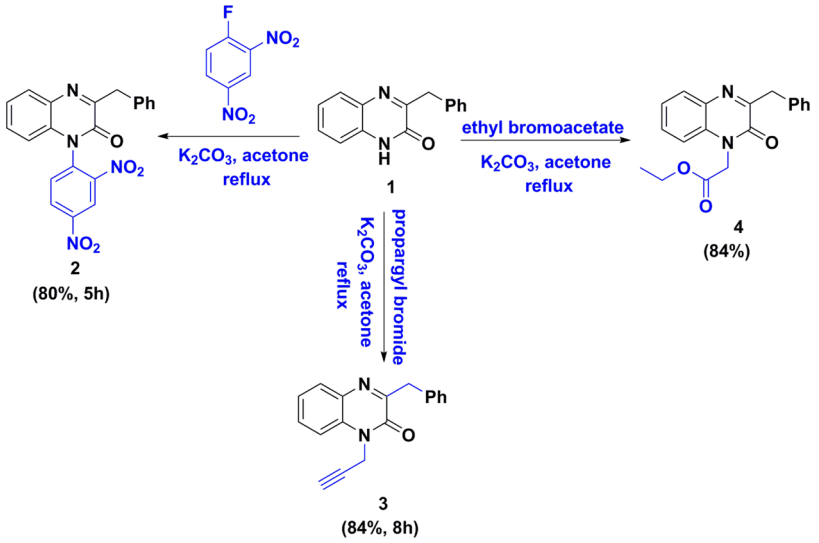

Scheme 2. Synthesis of N-Alkylated Quinoxaline Derivatives

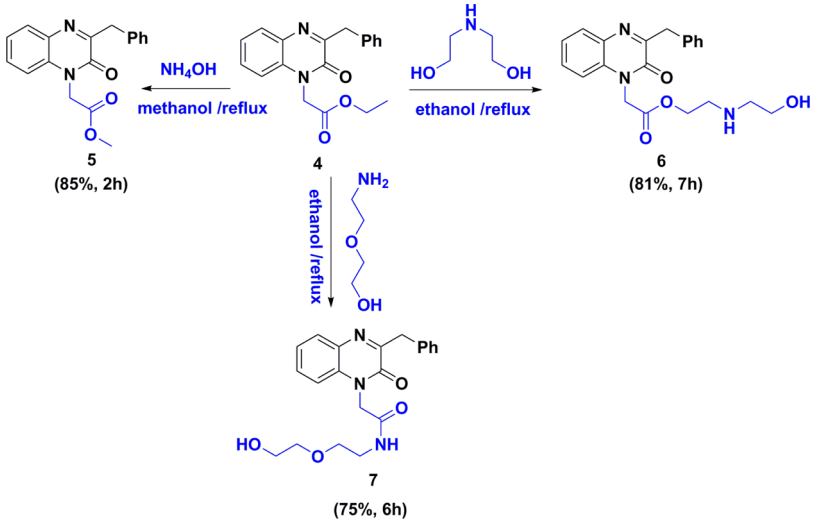

in methanol as the solvent afforded the corresponding methyl ester derivative **5** via transesterification instead of amidation. Furthermore, reflux of ester **4** with diethanolamine gives mono diethanolamine ester **6**. The reaction proceeds via transesterification rather than amidation. The formation of the long chain of the acetamide derivative was carried out by treatment of **4** with 2-(2-aminoethoxy) ethanol to afford the acyclo nucleoside analogue **7**. The structures of new compounds **5, 6**, and **7** were confirmed by using spectroscopic data. The structure of compound **5** was confirmed by the ^{1}H NMR spectrum and it exhibited a singlet peak at δ_H 3.68 ppm for C**H**$_3$ protons. In the ^{13}C NMR spectrum, compound **5** showed COO at δ_C: 168.0 ppm, whereas compound **6** showed six different separated peaks in the aliphatic region corresponding to six methylene groups at δ_H: 5.23, 4.12, 3.64, 3.56, 3.43, and 3.31, which confirm the asymmetry of the alkyl ester. Also NH and OH appeared at δ_H: 5.23 and 4.73 ppm, respectively, (exchangable with D_2O); also six signals of carbon in C NMR at δ_C: 59.1, 59.0, 50.1, 48.4, 44.4, and 39.4 (Ph**C**H$_2$, masked under solvent peaks). Compound **7** showed five different peaks at δ_C: 72.7, 69.4, 60.7, 60.6, and 45.1, which correspond to aliphatic **C**H$_2$'s carbon, 39.4 (Ph**C**H$_2$, masked under solvent peaks), and its ^{1}H NMR spectrum showed two exchangeable singlet peaks, one at δ_H 8.41 ppm attributed to NH and the second singlet at 2.86 ppm for OH (Scheme 2).

As adopted in Scheme 3, the hydrazinolysis of ester **4** was accomplished by treatment with hydrated hydrazine under reflux in the presence of absolute ethanol to afford the acid hydrazide derivative **8**.[20] Moreover, condensation of the latter with phthalic anhydride under reflux in glacial acetic acid afforded compound **9**.

Furthermore, the Schiff's base derivative **11** was prepared upon reflux of **8** with the monosodium salt of pyridoxal 5′-phosphate (P5P, **10**) in absolute ethanol. Elucidation of the structure of compound **9** was confirmed using ^{13}C NMR that presented three different signals revealing the carbonyls of isoindole, hydrazide, and imides at δ_C: 166.7, 165.4, and 159.2 ppm, respectively. Concerning compound **11**, the IR data showed bands at 3424 and 3324 cm^{-1} for OH and NH stretching; also, in the ^{1}H NMR spectrum, four peaks appeared at δ_H: 14.27, 12.05, 8.89, and 2.29 ppm representing O═P−**O**H, **O**H, **N**H, and C**H**$_3$ protons, respectively.

Moreover, compound **3** was employed as the starting material to synthesize a library of quinoxaline-triazole hybrid target

https://doi.org/10.1021/acsomega.4c01075
ACS Omega 2024, 9, 24643−24653

Scheme 3. Synthesis of Condensed Quinoxaline Derivatives

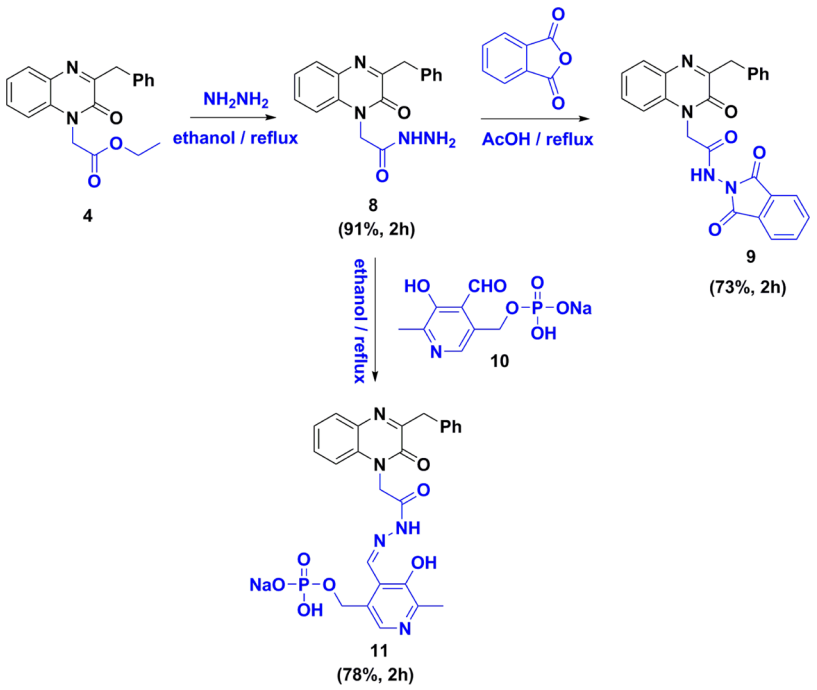

Scheme 4. Click Reaction Using Ethyl Azidobenzoate and Hydrolysis to Their Corresponding Acid

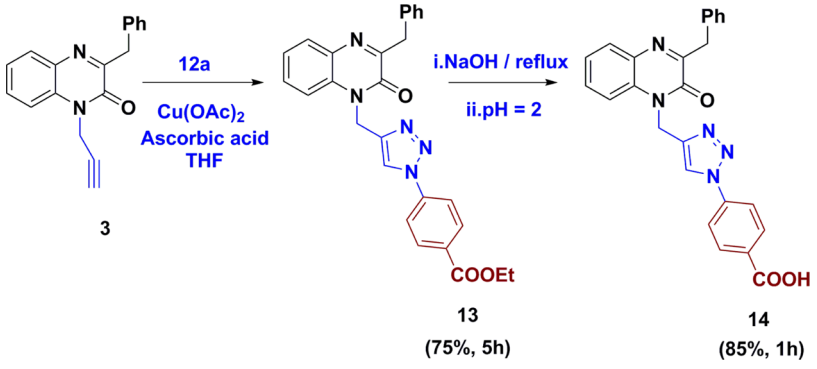

compounds (Figure 1) via click reaction[21] with different azides using a combination of $Cu(OAc)_2$ and ascorbate (Scheme 4). The reaction of compound **3** with ethyl 4-azidobenzoate (**12a**) afforded the quinoxaline-triazole hybrid ester **13**, which underwent the saponification reaction followed by treatment with HCl to give the corresponding benzoic acid derivative **14**. The structures of **13** and **14** were confirmed by using spectroscopic data; the IR spectrum of **13** revealed a strong band at 1719 cm^{-1} (COOEt); its ^1H NMR spectrum showed quartet and triplet peaks at δ_H: 4.28 and 1.28 ppm for CH_2 and CH_3 protons, respectively. Regarding compound **14**, two characteristic bands appearing in the IR spectrum at 3440 (OH) and 1780 (COOH) cm^{-1} were observed as strong bands. In order to create a range of quinoxaline-triazole hybrids for the purpose of studying the SARs, we treated compound 3 with various azides namely p-azidoiodobenzene, p-azidophenol, p-azidohippuric acid, p-azidoacetophenone, p-azidosulfacetamide, p-azidobenzenesulfanilamide, p-azidosulfaguanidine, or p-azidosulfadiazine **12b−i** respectively, in that order, to produce the hybrids **15−22**. The structures of these compounds were confirmed by spectroscopic analysis as reported in the Experimental section (Scheme 5).

2.2. Biological Evaluation. *2.2.1. Assessment of the Safe Concentrations of the New Compounds on Normal Colonic Epithelial Cells.* The newly synthesized compounds were tested for cytotoxicity against normal colonocytes to investigate the safety profile. The selectivity indices (SIs) were calculated, which is the measure of the selectivity of the drug candidate toward cancer cells rather than normal cells. When the SI is ≥3, the drug is highly selective; interestingly, most of them possessed remarkable selectivity; hence, compounds **6**, **9**, **14−18**, and **20** were found to be promising anticancer agents with SI values at the range 29.40−3.24 followed by compounds **2**, **7**, **19**, and **22** with SI values at 2.11−0.993. All of the compounds were safer than the reference doxorubicin (DOX, SI 0.357). Concerning EC100, all tested compounds, excluding **5**, **11**, **13**, and **21** showed a high safety profile on the growth of normal colonocytes with EC100 ≥ 0.1 μM[22−24] (Table 1).

2.2.2. Determination of Anticancer Activity on the Colorectal Cancer Cell Line (HCT-116). All of the prepared quinoxaline derivatives were tested for their anticancer potential on colorectal cancer cells (HCT-116) via MTT assay.[22−24] Generally, most of them showed promising anticancer activity (Table 1). Appealingly, compounds **6**, **9**, **14**, and **20** exhibited

https://doi.org/10.1021/acsomega.4c01075
ACS Omega 2024, 9, 24643−24653

Scheme 5. Synthesis of Quinoxaline-Triazole Derivatives 15−22

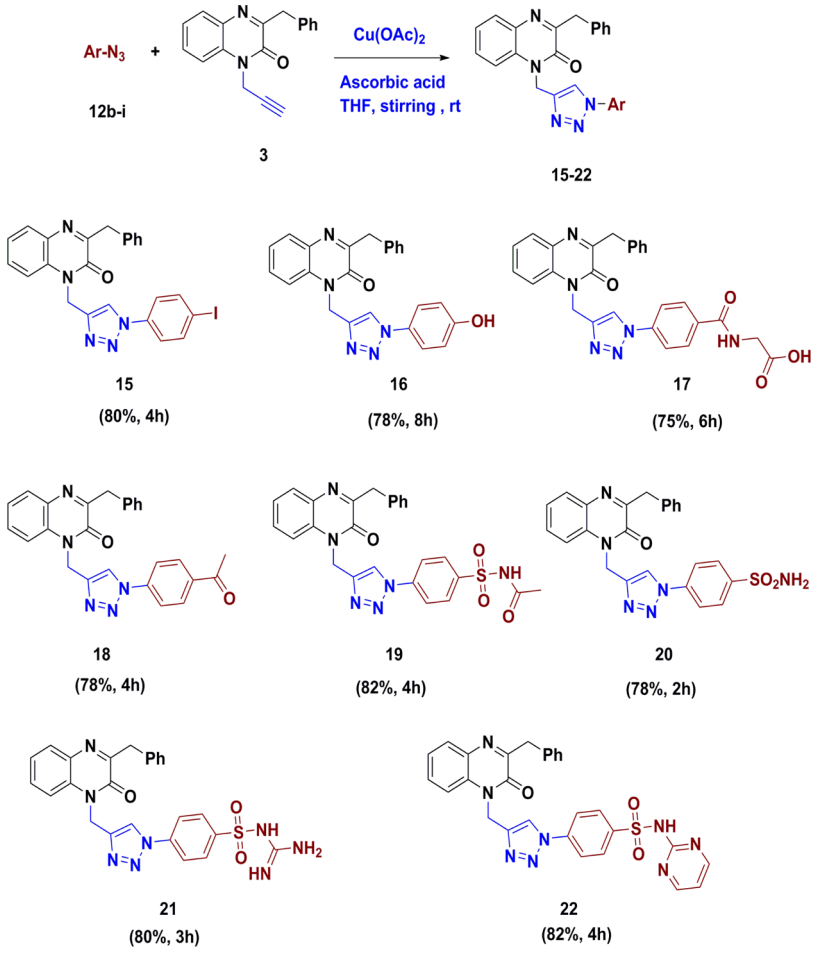

Table 1. Cytotoxicity and Selectivity Index (SI) Values of the Tested Quinoxalines[a]

	normal colonocyte		HCT-116	
compound	EC100 (μM)	IC_{50}-N (μM)	IC_{50} (μM)	SI
2	0.108 ± 0.013	0.462 ± 0.028	0.463 ± 0.032	0.998
5	0.080 ± 0.003	0.370 ± 0.074	0.438 ± 0.007	0.845
6	0.400 ± 0.078	1.676 ± 0.014	0.057 ± 0.009	29.404
7	0.170 ± 0.002	0.402 ± 0.060	0.405 ± 0.003	0.993
9	0.258 ± 0.018	0.444 ± 0.033	0.063 ± 0.013	7.048
11	0.034 ± 0.001	0.130 ± 0.012	0.123 ± 0.005	1.060
13	0.016 ± 0.002	0.052 ± 0.001	0.123 ± 0.001	0.423
14	0.265 ± 0.017	0.856 ± 0.018	0.055 ± 0.013	15.564
15	0.103 ± 0.008	0.438 ± 0.019	0.135 ± 0.009	3.244
16	0.556 ± 0.031	1.110 ± 0.078	0.222 ± 0.000	5.000
17	0.169 ± 0.036	0.372 ± 0.008	0.114 ± 0.001	3.263
18	0.212 ± 0.010	2.318 ± 0.021	0.218 ± 0.000	10.633
19	0.150 ± 0.015	0.401 ± 0.053	0.331 ± 0.004	1.211
20	0.193 ± 0.017	0.479 ± 0.014	0.072 ± 0.003	6.653
21	0.047 ± 0.006	0.115 ± 0.007	0.029 ± 0.013	3.966
22	0.124 ± 0.007	0.459 ± 0.021	0.217 ± 0.046	2.115
DOX	0.074 ± 0.008	0.272 ± 0.053	0.761 ± 0.050	0.357

[a]Values are demonstrated as mean ± SEM.

submicromolar IC_{50} 0.05−0.07 μM against HCT-116 cells within their safe dose (EC100), while DOX displayed IC_{50} 0.761 μM. These compounds exhibited selective cytotoxic activities against HCT-116 cells over normal colonocytes (SI; 29.4−6.6) compared to the other compounds and DOX (SI; 0.357). Compound **21** outperformed the other compounds in terms of IC_{50} (IC_{50}; 0.029 μM and SI; 3.96); nonetheless, we compromised between the selectivity index and cytotoxicity, for example. We chose the substances that showed strong anticancer activity along with excellent selectivity for further

https://doi.org/10.1021/acsomega.4c01075
ACS Omega 2024, 9, 24643−24653

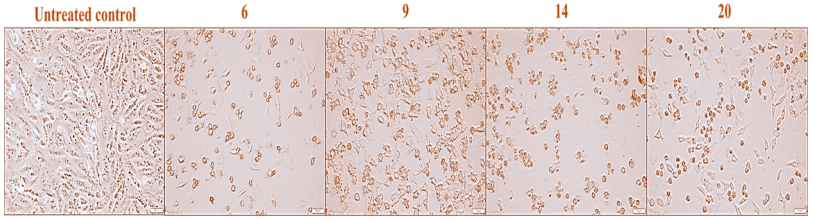

Figure 2. Morphological alterations of HCT-116 cells after 72 h of treatment of the most active compounds compared to the untreated cells.

Table 2. Relative Fold Change in the Gene Expression in the Treated HCT-116 Cells[a]

compd no.	HIF	VEGF	p21	BAX	p53	BCL-2
6	0.273 ± 0.002	0.497 ± 0.015	3.188 ± 0.035	4.114 ± 0.015	5.312 ± 0.012	0.213 ± 0.012
9	0.300 ± 0.011	0.512 ± 0.011	2.207 ± 0.082	3.041 ± 0.032	3.125 ± 0.078	0.561 ± 0.032
14	0.259 ± 0.006	0.395 ± 0.083	3.832 ± 0.080	4.321 ± 0.072	4.961 ± 0.042	0.143 ± 0.024
20	0.310 ± 0.002	0.615 ± 0.004	2.702 ± 0.188	3.565 ± 0.042	4.527 ± 0.063	0.347 ± 0.013

[a]All values are expressed as mean ± SEM.

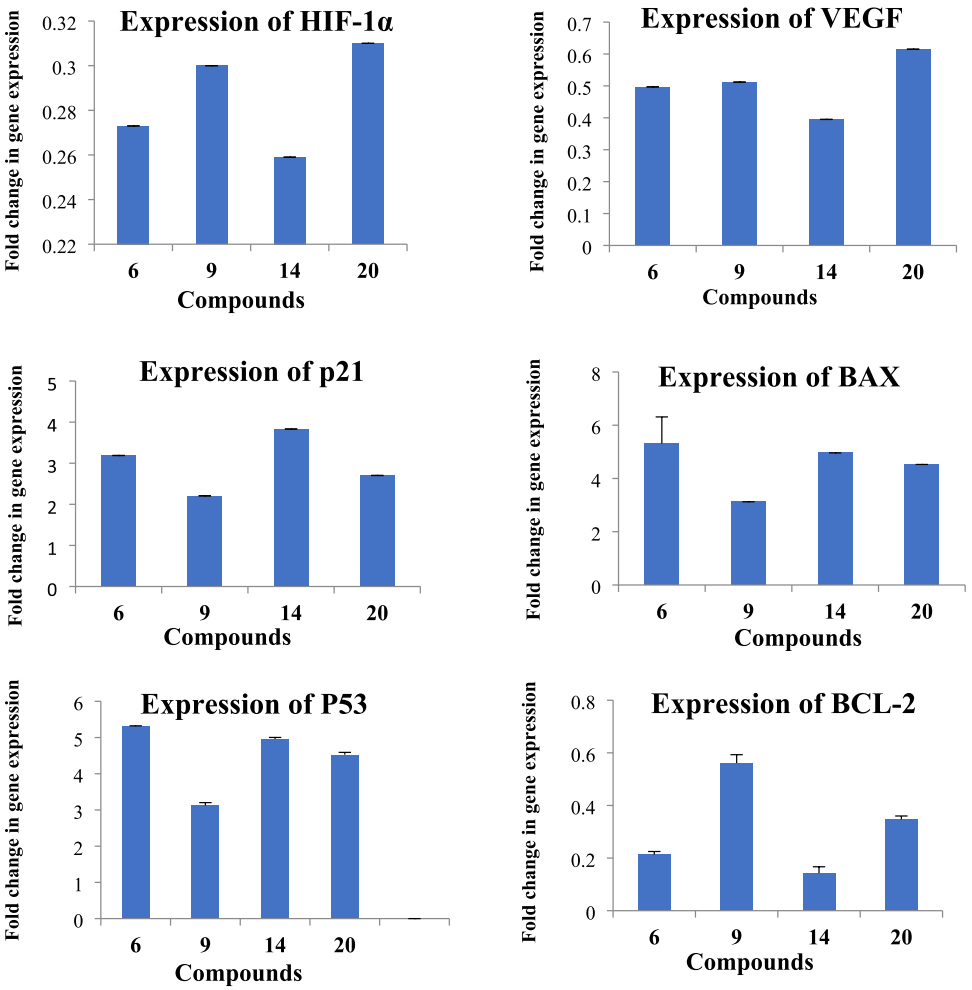

Figure 3. Effect of compounds **6**, **9**, **14**, and **20** on the relative gene expression of HIF, VEGF, p21, BAX, p53, and BCL-2.

mechanistic study. Obviously, compounds **6** and **14** were recognized as the most active compounds among the series, followed by the slightly less active derivatives **9** and then **20**. Compound **6** recorded the highest selectivity index (SI; 29.40) followed by **14** (SI; 15.56), **9** (SI; 7.04), and **20** (SI; 6.65).

2.2.3. Morphological Investigation of Promising Compounds in HCT-116. The most selective and potent hits, **6**, **9**, **14**, and **20**, were selected to be morphologically investigated for any changes occurring upon treatment with the colon cancer cell line (HCT-116) correlated to the untreated cancer cells (Figure 2). Obviously, all of the treated cells missed their original architecture. Furthermore, extreme shrinking appeared, designated dominant anticolon cancer activity of our hits, particularly compounds **6** and **14** compared to that of the untreated cancer cells.

https://doi.org/10.1021/acsomega.4c01075
ACS Omega 2024, 9, 24643−24653

Table 3. *In Silico* Physicochemical and Pharmacokinetic Properties of the Tested Compounds

compd no.	MLOGP[a]	M.Wt[b]	HBA[c]	HBD[d]	TPSA[e]	NROTB[f]	GI absorption	BBB permeation	Veber violations
2	2.86	402.36	6	0	126.53	5	high	no	0
5	1.62	293.32	3	1	77.98	4	high	no	0
6	1.33	381.43	6	2	93.45	10	high	no	0
7	0.93	381.43	5	2	93.45	10	high	no	0
9	2.80	438.43	5	1	101.37	6	high	no	0
11	0.28	559.44	10	3	175.04	11	low	no	2
13	3.91	493.56	6	0	91.90	8	high	no	0
14	3.18	437.45	6	1	102.90	6	high	no	0
15	4.22	519.34	4	0	65.60	5	high	yes	0
16	3.01	409.44	5	1	85.83	5	high	no	0
17	2.37	494.50	7	2	132.0	9	high	no	0
18	3.09	435.48	5	0	82.67	6	high	no	0
19	1.70	514.56	7	1	137.22	8	low	no	0
20	2.12	472.52	7	1	134.14	6	low	no	0
21	1.55	514.56	7	3	170.02	8	low	no	1
22	1.88	550.59	8	1	145.93	8	low	no	1

2.3. Structure–Activity Relationships. The preliminary SARS study has targeted the impact of pharmacophore moieties, the length of linkers used, and the distal moieties. Furthermore, it focused on both the electronic and hydrophobic nature of the substituents on the quinoxaline moiety. The SAR result displayed that the two types of quinoxalines, N^1-alkyl-/aralkylquinoxaline and quinoxaline-triazole hybrids, displayed different anticancer activity levels and possessed a distinctive pattern of selectivity against the HCT-116 cell line. However, the activity and selectivity were found to be a function of the substitution nature and size.

Among the evaluated N^1-alkylquinoxalines (**5**–**7**), the *N*-methyl acetate derivative **5** exhibited moderate activity. Chain extension of **5** gave two products (**6** and **7**); in the case of the ester, **6** unexpectedly conferred high cytotoxicity (IC_{50} 0.057 μM) against HCT-116 cells with an outstanding selectivity index (29.404). However, the other analogue **7** bearing ether in the side chain displayed an approximately similar activity to **5**. Notably, compound **9** (IC_{50} 0.063 μM) was among the most active compounds; the cytotoxicity is potentiated when the acetate side chain of **5** is attached to the lipophilic moiety (phthalimide).

Obviously, quinoxaline-triazole hybrids showed variable anticancer activities according to the aromatic ring substitution pattern attached to N^1-triazole. Interestingly, when the substituent is 4-benzoic acid in compound **14**, a potent anticancer activity (IC_{50} 0.055 μM) was demonstrated, while on masking the COOH group of **14** in the form of ester **13**, the activity was lessened (IC_{50}; 0.123 μM). Compound **14** is 2.2-fold more cytotoxic and 36.8-fold more selective and safer than its counterpart **13**. Replacing 4-benzoic acid in compound **14** with the isosteric moiety, benzenesulfonamide in compound **20** maintained the high potency (IC_{50}; 0.072 μM). On the contrary, the acetylation product (**19**) of compound **20** displayed a 4.6-fold lower anticancer activity. Concerning the halogenated derivative, the 4-iodophenyl derivative **15** exhibited a much lower activity than quinoxaline-triazole hybrids **14** and **20**. Thus, the lipophilic moiety is not recommended for colorectal cancer compared to the hydrophilic moiety of both hybrids, **14** (COOH) and **20** (SO_2NH_2).

2.4. qRT-PCR Analysis of HIF-1a, VEGF, p21, BAX, p53, and BCL-2 in HCT-116 Cells. Apoptosis is a developmentally preserved cell death mechanism that occurs in the adaptive cellular response to hypoxic stress. Apoptosis as well is a paramount safeguard against tumor growth. Based on the reports confirming that increased VEGF gene transcription is mediated by hypoxia-inducible factor-1*a* (HIF-1*a*),[25] the potent cytotoxic compounds **6**, **9**, **14**, and **20** were selected for examination by real-time PCR analyses to explore their regulatory potential on apoptosis's oncogenic mediators, HIF-1a, VEGF, and p21.[26−28] As shown in Table 2 and Figure 3, our hits can suppress gene expression of HIF-α and downstream gene VEGF; compound **14** revealed the highest potential to downregulate HIF-1α by 0.3-fold and inhibited the expression of VEGF by 0.4-fold in the treated HCT-116 cells. Furthermore, as indicated in literature,[25] the downregulation of VEGF by RNAi induces apoptosis, where p21 are important proteins associated with it. Therefore, we detected the levels of these apoptosis-associated proteins; notably, **14** revealed the highest ability to upregulate p21 by 3.83-fold, (Table 2, Figure 3). A correlation between the downregulation of both HIF-1α and VEGF and the upregulation of p21 expression was evident; thus, the activity order of our hits toward the tested oncogenic mediators was **14** > **6** > **9** > **20**.

The data presented above show that each compound has a significant effect on the expression levels of BAX, p53, and BCL-2. It is critical to add that the proteins were selected because of their important role in the modulation of apoptosis. Dysregulation of these proteins may lead to numerous diseases, particularly cancer. However, it may be noted that compound **6** and **14** mostly have a significant increase of BAX and p53 expression more than **9** and **20**. BAX is a proapoptotic protein, and its amounts escalate apoptosis. The tumor suppressor p53 controls cell cycle arrest and apoptosis. This suggests that these compounds induce apoptosis via a p53 mediator way. Furthermore, these compounds reduced the expression of BCL-2, an antiapoptotic protein, while the latter may suggest the proapoptotic effect of compounds. These findings provide insights into the potential therapeutic applications of these compounds in diseases involving dysregulated apoptosis such as cancer.

2.5. *In Silico* Studies. *2.5.1. Evaluation of Physicochemical and ADME Properties.* The physicochemical and *ADME* properties of the investigated compounds were determined utilizing computational study. *Swiss ADME*[29] software was applied to expect the bioactivity of the compounds related to

https://doi.org/10.1021/acsomega.4c01075
ACS Omega 2024, 9, 24643−24653

their critical parameters such as Lipinski and Veber rules. As delineated from Table 3, the physicochemical properties of most of the test compounds have zero Lipinski's violation. Also, most of them are in agreement with the parameters of Veber's rule.[29,30] This indicates that these derivatives have promising druglike properties. Compounds **11**, **21**, and **22** revealed Lipinski's violation due to MWt > 500; moreover, compound **11** has more violation, where NROTB > 10. Relying on the topological polar surface area (TPSA),[31] all compounds exhibit computational TPSA values in the appropriate range for permeating cell membranes except compounds **11**, **21**, and **22**, which have a poor polar surface area with PSA > 140 Å^2, which does not obey Veber's rule. It is apparent that all of the derivatives have high gastrointestinal absorption and can be used orally except **11** and **19**−**22**. Along with that, most of them have no permeation to the blood brain barrier, which outweighed that these systemically targeted molecules will have low to no CNS side effects.

Moreover, the prediction of drug-likeness and medicinal chemistry characters of the investigated compounds was accomplished by Swiss *ADME* software (Table 4). All

Table 4. Drug-Likeness and Medicinal Chemistry Parameters

compound	Lipinski's violation	bioavailability score	PAINS	synthetic accessibility
2	0	0.55	0	3.34
5	0	0.55	0	2.75
6	0	0.55	0	3.30
7	0	0.55	0	3.28
9	0	0.55	0	3.40
11	2	0.11	0	4.47
13	0	0.55	0	4.03
14	0	0.56	0	3.56
15	2	0.17	0	3.55
16	0	0.55	0	3.48
17	0	0.56	0	3.74
18	0	0.55	0	3.63
19	1	0.55	0	3.88
20	0	0.55	0	3.66
21	1	0.17	0	3.90
22	1	0.17	0	4.05

compounds have high scores of bioavailability (0.55) except compounds **11**, **15**, **21**, and **22** showing a bioavailability score of 0.11. Swiss *ADME* prediction revealed no alerts for all compounds. Overall, it could be established that the promising compounds presented acceptable medicinal chemistry parameters and drug-likeness values, which may introduce them as druglike candidates. *Swiss ADME* determined that all of the analogues had synthetic accessibility scores between 2.75 and 4.47, indicating that they can be easily synthesized on a large scale.

2.5.2. Molecular Docking Study. Types I and II of VEGFR-2 inhibitors can be distinguished based on their binding patterns. While type II inhibitors bind to both the ATP-binding site and the allosteric hydrophobic region, they have a higher degree of selectivity than type I inhibitors, which interact with the ATP-binding site and show reduced selectivity. The front and rear pockets constitute the basic design of the VEGFR-2 active site. The two essential residues that are linked to the ATP-binding front pocket are Glu917 and Cys919. The hydrophobic pocket at the rear contains Asp1046 and Glu885.[32] By interacting with the ATP-binding site in the catalytic domain of the receptor, VEGFR-2 inhibitors stop the dimerization and autophosphorylation processes of the receptor. As a result, the signaling cascade is prevented from starting, cell vascular permeability is reduced, and angiogenesis is eventually inhibited. Using MOE 2014 software, the known crystal structure of VEGFR-2 (PDB ID: 4ASD)[33] is used to investigate the binding interaction of target compounds. As a reference molecule, sorafenib, the cocrystallized ligand, was employed. The strongest VEGF expression inhibitors, our hits **6** and **14**, were docked in the VEGFR-2 active site. They exhibited significant affinity for VEGFR-2 when compared to the reference molecule, according to the results of docking tests. The cocrystallized ligand (sorafenib) was redocked against VEGFR-2 in order to verify the docking protocols. The implemented docking procedure was validated, as made evident by the obtained RMSD of 0.88.

The binding energy of the cocrystallized VEGFR-2 ligand, sorafenib, was −10.75 kcal/mol. Submerged in the ATP pocket, the heterocyclic system (the picolinamide moiety) formed two hydrogen bonds with Cys919 via nitrogen of the pyridine ring (bond length of 1.69 Å) and the carbonyl group (bond length of 2.48 Å). The urea moiety was positioned to make a hydrogen bond with Glu885 (bond length of 2.15 Å) in the rear hydrophobic pocket. Furthermore, urea's carbonyl and Asp1046 established a hydrogen connection with a bond length of 1.92 Å. Additionally, it formed many hydrophobic contacts with Lys868, Ala866, Glu885, Leu889, Leu1035, Cys1045, Phe1047, Asp1046, Val848, and Leu840.

In general, the most important residues in the binding site, Glu885, Glu917, Asp1046, Cys919, Cys1045, and Lys868, were successfully attached to our compounds. The docked model of compound **6** demonstrated a docking score energy of −11.41 kcal/mol, which is superior to that of sorafenib. It forms two hydrogen bonds, the longest of which is 3.30 Å, and connects the methylene group to Glu885, the reference drug, in the rear hydrophobic pocket. Between the carbonyl group of the quinoxaline nucleus and the Lys868 residue, another hydrogen bond with a length of 2.60 Å is created. It also showed three arene-H interactions. The phenyl ring and residues Asp1046 and Cys1045 were shown to have two arene-H interactions, whereas the quinoxaline moiety and Cys1045 create the final one. Specifically, our hit's hydrophobic interactions with Asp814, Val848, Lys868, Ile888, Leu889, Glu885, Val916, Leu1019, His1026, Cys1045, Asp1046, and His1026 were found (Figure 4).

In comparison to sorafenib, our hit **14** showed an extremely low free binding energy of −13.11 kcal/mol. Through two H-bond interactions in the hinge region (bond lengths of 2.99 and 2.11 Å, respectively, between the carboxylic group and Cys919 and Glu917), the interaction blocks the ATP pocket. Additionally, Leu840 is linked to the triazole moiety as a linker by an arene-H interaction. Additionally, a great deal of hydrophobic interactions with Gly922, Phe1047, Leu840, Leu1035, and Phe918 was noted (Figure 4).

3. CONCLUSIONS

This study demonstrates the design and synthesis of new N^1-substituted quinoxaline and quinoxaline-triazole hybrids; most of the compounds displayed anticancer activity with variable ratios. Overall, the MTT assay results highlighted the promising anticancer activity of the quinoxaline-triazole hybrids, specifically compounds **6**, **9**, **14**, and **20**, against colorectal cancer cells. These compounds exhibited significant cytotoxicity, maintained

https://doi.org/10.1021/acsomega.4c01075
ACS Omega 2024, 9, 24643−24653

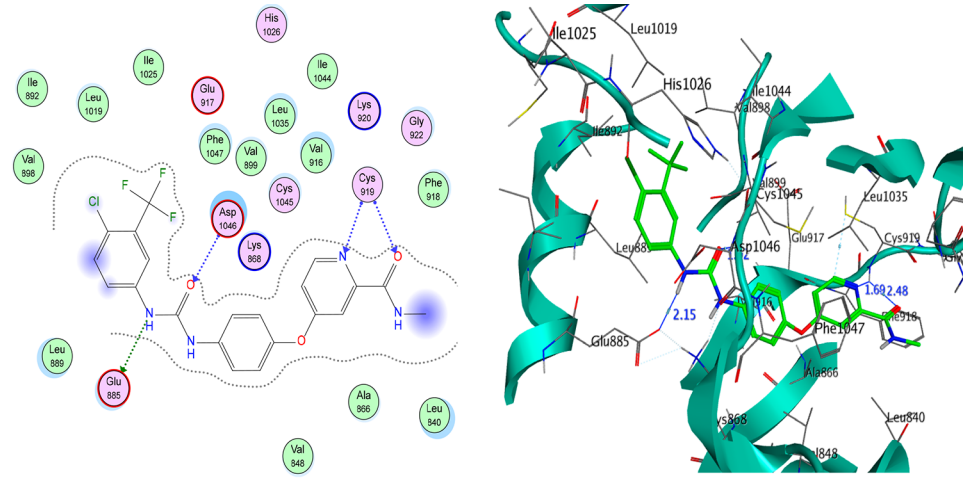

2D and 3D of Sorafenib Energy -10.75 Kcal/mol

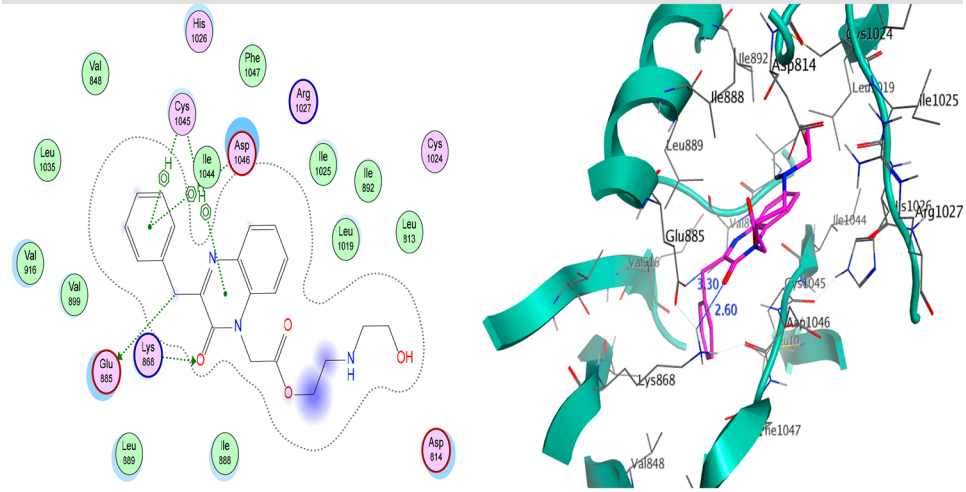

2D and 3D of compound **6** Energy -11.41 Kcal/mol

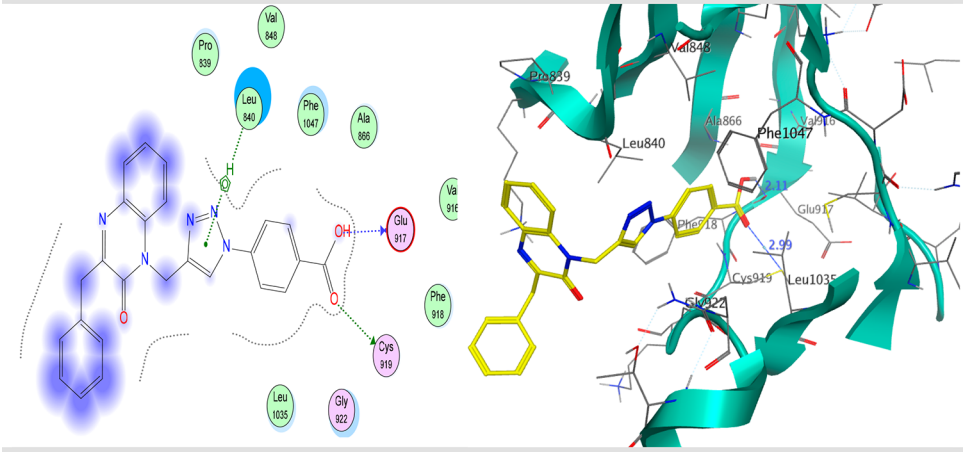

2D and 3D of compound **14** Energy -13.11 Kcal/mol

Figure 4. Docked pose of sorafenib and compounds **6** and **14** in the VEGFR-2 active site.

selectivity toward cancer cells while sparing normal colonocytes, and induced morphological alterations and shrinkage in treated cancer cells. Clearly, they were the safest ones, exhibiting the highest selectivity profiles compared to doxorubicin. The qRT-PCR analysis further elucidated the potential molecular mechanisms underlying the observed anticancer activities involving the modulation of HIF-1α, VEGF, and p21 gene expression. Therefore, compounds **6**, **9**, **14**, and **20** were selected for further mechanistic studies where they exhibited the downregulation of HIF-1a, VEGF, and BCL-2. They enhanced

https://doi.org/10.1021/acsomega.4c01075
ACS Omega 2024, 9, 24643−24653

the proapoptotic gene expression of p21, p53, and BAX in HCT-116 cells as well. *In silico* prediction revealed that most of them comply with Lipinski and Veber rules with acceptable medicinal chemistry and drug-likeness parameters. Docking tests confirmed our suggested mechanism of action for **6** and **14** as VEGFR-2 inhibitors and showed virtually the same binding manner compared to the reference drug sorafenib.

4. EXPERIMENTAL SECTION

4.1. Materials and Equipment. The material and equipment characterization are reported in the Supporting Information.

4.2. Synthesis of Compounds 2−22. The synthetic procedures, explanations of the NMR data, and copy of ^{1}H NMR and ^{13}C NMR are reported in the Supporting Information file.

4.3. Biological Evaluation. *4.3.1. Cytotoxicity Screening on Normal Colon Cells.* The normal colonic epithelial cells were isolated utilizing the Follmann & Birkner method[22] with modifications[23] and the cytotoxicity evaluation of the novel compounds were tested via MTT assay[24] as mentioned in the Supporting Information Data.

4.3.2. Anticancer Evaluation on HCT-116. The anticancer evaluation of the tested compounds was performed via MTT assay[24] and the procedure is detailed in the Supporting Information Data.

4.3.3. qRT-PCR Analysis of HIF-1a, VEGF, and p21 in HCT-116. After treatment of HCT-116 cells with the most active anticancer compounds for 72 h, qRT-PCR analysis was performed for HIF-1a[6,34] as detailed in the Supporting Information Data.

4.3.4. Statistical Analysis.[35] The data are expressed as mean ± standard error of mean (SEM) and the significant values were considered at $p < 0.05$. One-way analysis of variance (ANOVA) by Tukey's test was used for evaluating the difference between the mean values of the studied treatments. The analysis was done for three measurements using SPSS software version 16.

■ ASSOCIATED CONTENT

Data Availability Statement

All data that support the findings of this study are available online.

Supporting Information

The Supporting Information is available free of charge at https://pubs.acs.org/doi/10.1021/acsomega.4c01075.

Experimental procedures of the biological evaluation; synthesis of the target compounds; explanation of the spectral data; and copy of ^{1}H NMR and ^{13}C NMR (PDF)

■ AUTHOR INFORMATION

Corresponding Authors

Mohammed Salah Ayoup − *Department of Chemistry, College of Science, King Faisal University, Al-Ahsa 31982, Saudi Arabia; Chemistry Department, Faculty of Science, Alexandria University, Alexandria 21321, Egypt;* orcid.org/0000-0001-6715-5478; Email: mayoup@kfu.edu.sa

Adel Amer − *Chemistry Department, Faculty of Science, Alexandria University, Alexandria 21321, Egypt;* Email: adel.amer@alex-sci.edu.eg

Authors

Ahmed R. Rabee − *Chemistry Department, Faculty of Science, Alexandria University, Alexandria 21321, Egypt*

Hamida Abdel-Hamid − *Chemistry Department, Faculty of Science, Alexandria University, Alexandria 21321, Egypt*

Marwa M. Abu-Serie − *Medical Biotechnology Department, Genetic Engineering and Biotechnology Research Institute, City of Scientific Research and Technological Applications (SRTA-City), Alexandria 21934, Egypt*

Samah Ashraf − *Bio-screening and Preclinical Trial Lab, Biochemistry Department, Faculty of Science, Alexandria University, 21511 Alexandria, Egypt*

Doaa A. Ghareeb − *Bio-screening and Preclinical Trial Lab, Biochemistry Department, Faculty of Science, Alexandria University, 21511 Alexandria, Egypt; Center of Excellence for Drug Preclinical Studies (CE-DPS), Pharmaceutical and Fermentation Industry Development Center, City of Scientific Research & Technological Applications (SRTA-city), Alexandria 21934, Egypt;* orcid.org/0000-0003-3327-4377

Rabab S. Ibrahim − *Department of Pharmaceutical Medicinal Chemistry and Drug Design, Faculty of Pharmacy (Girls), Al-Azhar University, Cairo 11754, Egypt*

Mohammed B. Hawsawi − *Department of Chemistry, Faculty of Science, Umm Al-Qura University, Makkah 24382, Saudi Arabia;* orcid.org/0000-0003-1527-5560

Amr Negm − *Department of Chemistry, College of Science, King Faisal University, Al-Ahsa 31982, Saudi Arabia; Chemistry Department, Faculty of Science, Mansoura University, Mansoura 35516, Egypt;* orcid.org/0000-0001-9801-3261

Magda M. F. Ismail − *Department of Pharmaceutical Medicinal Chemistry and Drug Design, Faculty of Pharmacy (Girls), Al-Azhar University, Cairo 11754, Egypt*

Complete contact information is available at: https://pubs.acs.org/10.1021/acsomega.4c01075

Notes

The authors declare no competing financial interest.

■ ACKNOWLEDGMENTS

The authors acknowledge the Deanship of Scientific Research, Vice Presidency for Graduate Studies and Scientific Research at King Faisal University, Saudi Arabia, for financial support under the annual funding track (Project No. GrantA246).

■ REFERENCES

(1) Carnahan, L. R.; Jones, L.; Brewer, K. C.; Watts, E. A.; Peterson, C. E.; Ferrans, C. E.; Cipriano-Steffens, T.; Polite, B.; Maker, A. V.; Chowdhery, R.; et al. Race and gender differences in awareness of colorectal cancer screening tests and guidelines among recently diagnosed colon cancer patients in an urban setting. *J. Cancer Educ.* **2021**, *36*, 567−575.

(2) Zonta, Y. R.; Martinez, M.; Camargo, I. C. C.; Domeniconi, R. F.; Lupi Júnior, L. A.; Pinheiro, P. F. F.; Reiter, R. J.; Martinez, F. E.; Chuffa, L. G. A. Melatonin reduces angiogenesis in serous papillary ovarian carcinoma of ethanol-preferring rats. *Int. J. Mol. Sci.* **2017**, *18* (4), 763.

(3) Liu, L.; Qin, S.; Zheng, Y.; Han, L.; Zhang, M.; Luo, N.; Liu, Z.; Gu, N.; Gu, X.; Yin, X. Molecular targeting of VEGF/VEGFR signaling by the anti-VEGF monoclonal antibody BD0801 inhibits the growth and induces apoptosis of human hepatocellular carcinoma cells in vitro and in vivo. *Cancer Biol. Ther.* **2017**, *18* (3), 166−176.

(4) Shibata, A.; Nakagawa, K.; Sookwong, P.; Tsuduki, T.; Oikawa, S.; Miyazawa, T. δ-Tocotrienol Suppresses VEGF Induced Angiogenesis whereas α-Tocopherol Does Not. *J. Agric. Food Chem.* **2009**, *57* (18), 8696−8704.
(5) Germain, S.; Monnot, C.; Muller, L.; Eichmann, A. Hypoxia-driven angiogenesis: role of tip cells and extracellular matrix scaffolding. *Curr. Opin. Hematol.* **2010**, *17* (3), 245−251.
(6) Maxwell, P. H.; Pugh, C. W.; Ratcliffe, P. J. Activation of the HIF pathway in cancer. *Curr. Opin. Genet. Dev.* **2001**, *11* (3), 293−299.
(7) Vaupel, P.; Mayer, A. Hypoxia in cancer: significance and impact on clinical outcome. *Cancer Metastasis Rev.* **2007**, *26*, 225−239.
(8) Zengin, M.; Tan, O. U.; Arafa, R. K.; Balkan, A. Design and synthesis of new 2-oxoquinoxalinyl-1, 2, 4-triazoles as antitumor VEGFR-2 inhibitors. *Bioorg. Chem.* **2022**, *121*, No. 105696.
(9) Imanishi, M.; Sonoda, M.; Miyazato, H.; Sugimoto, K.; Akagawa, M.; Tanimori, S. Sequential Synthesis, Olfactory Properties, and Biological Activity of Quinoxaline Derivatives. *ACS Omega* **2017**, *2* (5), 1875−1885.
(10) El-Tombary, A.; AM El-Hawash, S. Synthesis, antioxidant, anticancer and antiviral activities of novel quinoxaline hydrazone derivatives and their acyclic C-nucleosides. *Med. Chem.* **2014**, *10* (5), 521−532.
(11) Montana, M.; Montero, V.; Khoumeri, O.; Vanelle, P. Quinoxaline derivatives as antiviral agents: a systematic review. *Molecules* **2020**, *25* (12), 2784.
(12) Ayoup, M. S.; Ammar, A.; Abdel-Hamid, H.; Amer, A.; Abu-Serie, M. M.; Nasr, S. A.; Ghareeb, D. A.; Teleb, M.; Tageldin, G. N. Challenging the anticolorectal cancer capacity of quinoxaline-based scaffold via triazole ligation unveiled new efficient dual VEGFR-2/MAO-B inhibitors. *Bioorg. Chem.* **2024**, *143*, No. 107102.
(13) El-Adl, K.; Sakr, H. M.; Yousef, R. G.; Mehany, A. B.; Metwaly, A. M.; Elhendawy, M. A.; Radwan, M. M.; ElSohly, M. A.; Abulkhair, H. S.; Eissa, I. H. Discovery of new quinoxaline-2 (1H)-one-based anticancer agents targeting VEGFR-2 as inhibitors: Design, synthesis, and anti-proliferative evaluation. *Bioorg. Chem.* **2021**, *114*, No. 105105.
(14) Osmaniye, D.; Baltacı Bozkurt, N.; Levent, S.; Benli Yardımcı, G.; Sağlık, B. N.; Ozkay, Y.; Kaplancıklı, Z. A. Synthesis, Antifungal Activities, Molecular Docking and Molecular Dynamic Studies of Novel Quinoxaline-Triazole Compounds. *ACS Omega* **2023**, *8* (27), 24573−24585.
(15) El Rayes, S. M.; Aboelmagd, A.; Gomaa, M. S.; Ali, I. A. I.; Fathalla, W.; Pottoo, F. H.; Khan, F. A. Convenient Synthesis and Anticancer Activity of Methyl 2-[3-(3-Phenyl-quinoxalin-2-ylsulfanyl)-propanamido]alkanoates and N-Alkyl 3-((3-Phenyl-quinoxalin-2-yl)-sulfanyl)propanamides. *ACS Omega* **2019**, *4* (20), 18555−18566.
(16) Khattab, S. N.; Hassan, S. Y.; Bekhit, A. A.; El Massry, A. M.; Langer, V.; Amer, A. Synthesis of new series of quinoxaline based MAO-inhibitors and docking studies. *Eur. J. Med. Chem.* **2010**, *45* (10), 4479−4489.
(17) Ayoup, M. S.; Rabee, A. R.; Abdel-Hamid, H.; Harras, M. F.; El Menofy, N. G.; Ismail, M. M. Exploration of Nitroaromatic Antibiotics via Sanger's Reagent: Synthesis, In Silico, and Antimicrobial Evaluation. *ACS Omega* **2022**, *7* (6), 5254−5263.
(18) Ayoup, M. S.; Abu-Serie, M. M.; Awad, L. F.; Teleb, M.; Ragab, H. M.; Amer, A. Halting colorectal cancer metastasis via novel dual nanomolar MMP-9/MAO-A quinoxaline-based inhibitors; design, synthesis, and evaluation. *Eur. J. Med. Chem.* **2021**, *222*, No. 113558.
(19) Khattab, S. N.; Moneim, S. A. A.; Bekhit, A. A.; El Massry, A. M.; Hassan, S. Y.; El-Faham, A.; Ahmed, H. E. A.; Amer, A. Exploring new selective 3-benzylquinoxaline-based MAO-A inhibitors: design, synthesis, biological evaluation and docking studies. *Eur. J. Med. Chem.* **2015**, *93*, 308−320.
(20) Khattab, S. N.; Abdel Moneim, S. A. H.; Bekhit, A. A.; El Massry, A. M.; Hassan, S. Y.; El-Faham, A.; Ali Ahmed, H. E.; Amer, A. Exploring new selective 3-benzylquinoxaline-based MAO-A inhibitors: Design, synthesis, biological evaluation and docking studies. *Eur. J. Med. Chem.* **2015**, *93*, 308−320.
(21) Ayoup, M. S.; Cordes, D. B.; Slawin, A. M. Z.; O'Hagan, D. Selectively fluorinated cyclohexane building blocks: Derivatives of carbonylated all-cis-3-phenyl-1,2,4,5-tetrafluorocyclohexane. *Beilstein J. Org. Chem.* **2015**, *11*, 2671−2676.
(22) Föllmann, W.; Weber, S.; Birkner, S. Primary cell cultures of bovine colon epithelium: isolation and cell culture of colonocytes. *Toxicol. in Vitro* **2000**, *14* (5), 435−445.
(23) Abu-Serie, M. M.; El Demellawy, M. A.; El-Sayed, M.; El-Rashidy, F. In vitro sustained differentiation of rat colon epithelial stem cells. *Biochem. Anal. Biochem.* **2016**, *05* (239), No. 2161-1009, DOI: 10.4172/2161-1009.1000239.
(24) Mosmann, T. Rapid colorimetric assay for cellular growth and survival: application to proliferation and cytotoxicity assays. *J. Immunol. Methods* **1983**, *65* (1−2), 55−63.
(25) Sun, P.; Yu, H.; Zhang, W.-Q.; Hu, M.; Lv, R. Lentivirus-mediated siRNA targeting VEGF inhibits gastric cancer growth in vivo. *Oncol. Rep.* **2012**, *28* (5), 1687−1692.
(26) Colwell, N.; Larion, M.; Giles, A. J.; Seldomridge, A. N.; Sizdahkhani, S.; Gilbert, M. R.; Park, D. M. Hypoxia in the glioblastoma microenvironment: shaping the phenotype of cancer stem-like cells. *Neuro-Oncology* **2017**, *19* (7), 887−896.
(27) Jiang, X.; Huang, Y.; Wang, X.; Liang, Q.; Li, Y.; Li, F.; Fu, X.; Huang, C.; Liu, H. Dianhydrogalactitol, a potential multitarget agent, inhibits glioblastoma migration, invasion, and angiogenesis. *Biomed. Pharmacother.* **2017**, *91*, 1065−1074.
(28) Zhang, F.; Shi, J.-J.; Thakur, K.; Hu, F.; Zhang, J.-G.; Wei, Z.-J. Anti-cancerous potential of polysaccharide fractions extracted from peony seed dreg on various human cancer cell lines via cell cycle arrest and apoptosis. *Front. Pharmacol.* **2017**, *8*, No. 102.
(29) Daina, A.; Michielin, O.; Zoete, V. SwissADME: a free web tool to evaluate pharmacokinetics, drug-likeness and medicinal chemistry friendliness of small molecules. *Sci. Rep.* **2017**, *7* (1), No. 42717.
(30) Veber, D. F.; Johnson, S. R.; Cheng, H.-Y.; Smith, B. R.; Ward, K. W.; Kopple, K. D. Molecular properties that influence the oral bioavailability of drug candidates. *J. Med. Chem.* **2002**, *45* (12), 2615−2623.
(31) Maximo da Silva, M.; Comin, M.; Santos Duarte, T.; Foglio, M. A.; De Carvalho, J. E.; do Carmo Vieira, M.; Nazari Formagio, A. S. Synthesis, antiproliferative activity and molecular properties predictions of galloyl derivatives. *Molecules* **2015**, *20* (4), 5360−5373.
(32) Rampogu, S.; Baek, A.; Zeb, A.; Lee, K. W. Exploration for novel inhibitors showing back-to-front approach against VEGFR-2 kinase domain (4AG8) employing molecular docking mechanism and molecular dynamics simulations. *BMC Cancer* **2018**, *18* (1), No. 264.
(33) Abdallah, A. E.; Mabrouk, R. R.; Al Ward, M. M. S.; Eissa, S. I.; Elkaeed, E. B.; Mehany, A. B.; El-Zahabi, M. A.; et al. Synthesis, biological evaluation, and molecular docking of new series of antitumor and apoptosis inducers designed as VEGFR-2 inhibitors. *J. Enzyme Inhib. Med. Chem.* **2022**, *37* (1), 573−591.
(34) Li, C.; Wang, Q.; Shen, S.; Wei, X.; Li, G. HIF-1α/VEGF signaling-mediated epithelial-mesenchymal transition and angiogenesis is critically involved in anti-metastasis effect of luteolin in melanoma cells. *Phytother. Res.* **2019**, *33* (3), 798−807.
(35) Ostertagová, E.; Ostertag, O. Methodology and Application of One-way ANOVA. *Am. J. Mech. Eng.Engineering* **2013**, *1* (7), 256−261.

https://doi.org/10.1021/acsomega.4c01075
ACS Omega 2024, 9, 24643−24653